Journal of Engineering Science and Technology
Vol. 13, No. 10 (2018) 3297 - 3312
© School of Engineering, Taylor's University

MULTI-RESPONSE OPTIMIZATION OF PROCESS PARAMETERS BY TAGUCHI GREY RELATIONAL ANALYSIS FOR DISSIMILAR THICKNESS FRICTION STIR PROCESS CORNER WELD AA5086 ALLOY

MANIGANDAN KRISHNAN*, SENTHILKUMAR SUBRAMANIAM

School of Mechanical Engineering, VIT University, Vellore, India
*Corresponding Author: manikvit@gmail.com

Abstract

This paper presents the multi-response optimization of friction stir corner welding process for dissimilar thickness AA5086 aluminium alloy plates. The corner joint of AA5086 aluminium alloy plates of thicknesses of 6 mm and 4 mm was welded by Friction Stir Welding (FSW) process. The FSW experiments were conducted agreeing to the L_9 orthogonal array. Three FSW process parameters: tool traverse speed (100, 150 and 190 mm/min), rotational speed (900, 1000 and 1100 rev/min), and plunge depth (0.1, 0.2, and 0.3 mm) were related with weld tensile strength and hardness. The Analysis of Variance (ANOVA) was used to determine the percentage contribution of each input parameter on the weld quality. Taguchi Grey Relational Analysis is used to optimize and order the FSW process parameters. Conferring to the results of the analyses, the optimal welding condition was determined as 1000 rev/min for tool rotational speed, 150 mm/min for traverse speed and 0.1 mm for tool plunge depth. The percentage contribution of the traverse speed (54%) revealed a significant influence compared to tool rotational speed (21%) and plunge depth (13%). The microstructures of various zones were observed and analysed. Tensile tests were conducted and the fracture was observed at heat affected zones for all the joints. Current consumption, temperature distribution, and force generation during friction stir welding were acquired and analysed.

Keywords: Corner joint, Dissimilar thickness, Friction stir welding, Microstructure, Optimization.

1. Introduction

Aluminium alloy materials were difficult to weld by fusion welding processes and numerous welding defects, like voids, hot cracking, distortion, lack of penetration occur in traditional fusion welding of aluminium alloys. The problems could overcome by Friction stir welding (FSW), which is a solid-state welding process invented by W. Thomas of The Welding Institute (TWI), The United Kingdom in 1991 [1]. The maximum temperature produced during welding is less than 80% of the melting temperature of parent material. A non-consumable rotating tool is plunged between plates to be welded with adequate vertical force and travelled along the weld line. The FSW tool contains shoulder and a pin. Tool shoulder generates frictional heat that softens the materials around the tool pin. The plasticized material was pushed to rear from front of the tool pin by transverse movement of the tool and forges to carry out the welding process. FSW is appropriate to weld non-ferrous metals, such as aluminium, copper, titanium, magnesium, and attempts have been made to weld steel and dissimilar metals.

AA5086 is a non-heat treatable aluminium alloy exhibits higher strength to weight ratio, good ductility, and good corrosion resistance. It is widely used to fabricate marine and transportation equipment. FSW is successfully applied for different joint designs such as butt, lap, tee and corner joints. The corner joint is a joint in which, two metal parts to be welded are retained with a right angle to one another, which is considered in this study. Good amounts of researches have been carried out on FSW of butt joints. Yan et al. [1] studied dissimilar friction stir welding between 5052 aluminium alloy and AZ31 magnesium alloy and observed the uneven distribution of microhardness profile and it was found two times higher than the base material at the weld zone. The rotational speed of 600 rev/min and the transverse speed of 40 mm/min produced the sound weld. Ilangovan et al. [2] analysed the effect of tool pin profile on microstructure and tensile properties of friction stir welded dissimilar AA6061/AA5086 aluminium alloy joints. It was observed that the better performance of welds produced by threaded pin profiled tool and caused finer and uniform distribution of grains, onion rings and finer grain. The traverse speed plays a vital role in the formation of the plastically deformed region.

Palanivel et al. [3] found that the better tensile properties were obtained in the weld fabricated at a traverse speed of 63 mm/min. Ahmed et al. [4] studied FSW of similar and dissimilar AA7075 and AA5083 materials. The joints revealed ultimate tensile strength between 245 and 267 MPa with joint efficiency between 77 and 87% to the strength of AA5083 parent metal. Martin et al. [5] presented the techniques for welding corner joints using FSW. The corner joints were fabricated by FSW using stationary shoulder rotating tool with AA6082-T6 filler material. The joints produced in the AA5083-O alloy failed at parent material irrespective of the filler material used. The heat treatable alloy AA6061 in both tests failed at heat affected zones. The maximum tensile strength obtained for AA5083-O joint was 310 MPa. Palanivel and Mathew [6] performed the optimization of a process parameter of FSW AA5083 aluminium alloy using Response Surface Methodology. The maximum ultimate tensile strength value of the weld was 260 MPa. The better mechanical properties were obtained with process parameters of the rotational speed at 1000 rev/min and traverse speed at 69 mm/min. Casalino et al. [7] studied the influence of too shoulder geometry and coating of the tool on the FSW of aluminium alloy plates. The shoulder size influences size of the

microstructure zone and the hardness profile. The large shoulder coated with carbide produced defect-free welds.

Sahu and Pal [8] carried out multi-response optimization of process parameters in friction stir welded AM20 magnesium alloy by Taguchi Grey Relational Analysis and observed that the most influenced parameters were traverse speed and shoulder diameter, then the optimum parameters were 0.12 mm of plunge depth, 1100 rev/min of tool rotational speed, 98 mm/min of traverse speed, and shoulder diameter of 24 mm.

There is limited literature on the study of FSW AA5086 plates with corner joint. An attempt has been made to optimize the multiple quality characteristics of friction stir welded AA5086 aluminium alloy using Taguchi Grey Relational Analysis technique. The process parameters are optimized based on output responses of mechanical properties and uncontrollable noise factors such as the ultimate tensile strength, average hardness at different zones, joint efficiency maximum temperature distribution, maximum current consumption, and maximum force generation. The most influenced input parameter was determined by analysing the grey relational grades and percentage contribution of process parameters were also determined using Analysis of Variance (ANOVA).

2. Materials and Methods

Aluminium alloy AA5086 was used as parent material in this work. The mechanical properties and chemical composition of the AA5086 alloy are given in Table 1.

Table 1. Mechanical properties of AA5086 aluminium alloy.

Mechanical property	AA5086
Yield strength	212 MPa
Ultimate tensile strength	250 MPa
Elongation	21%

FSW work plates with dimensions of 100 mm × 50 mm × 6 mm (vertical) and 100 mm × 50 mm × 4 mm (horizontal) were prepared from the rolled plates. A cylindrical threaded pin FSW tool with 18 mm of shoulder diameter and 3.7 mm length of the cylindrical pin was used for welding experiments. The tool was machined from D2 tool steel and heat-treated to 58 HRC. The friction stir welding experiments of corner joint were carried out using the modified vertical milling machine (HMT-INDIA) as shown in Fig. 1. The schematic diagram of dissimilar thickness friction stir welding corner joint is shown in Fig. 2. The chemical composition of the AA5086 alloy is Cr-0.05%, Cu-0.1%, Fe-0.5%, Mg-3.5%, Mn-0.2%, Si-0.4%, Ti-0.15%, Zn-0.25%, and Al-Balance.

The fixture used for locating and clamping the weld work plates during corner welding is shown in Fig. 3. The preliminary experiments carried out with tool rotational speed less than 900 rev/min generated tunnel defects in the weld joint, due to the inadequate heat generation, material transformation and welding above 1100 rev/min defect produced due to excessive turbulence. Besides, the welding traverse speeds below 100 mm/min and beyond 190 mm/min caused defects in the entire length of joints with a rough surface. If the plunge depth increased more than 0.3 mm, the edge of the pin contacted the backing bar of the fixture during welding because the thickness of the material is 4 mm and pin length is 3.7 mm. The plunge

depth less than 0.1 mm could not produce adequate plastic deformation and frictional heat results in tunnel defect at bottom of the weld. From the observations, the ranges of tool rotational speed from 900 rev/min to 1100 rev/min, welding speed from 100 mm/min to 190 mm/min and plunging depth from 0.1 mm to 0.3 mm were considered to conduct the FSW experiments.

Fig. 1. Vertical milling machine with FSW setup.

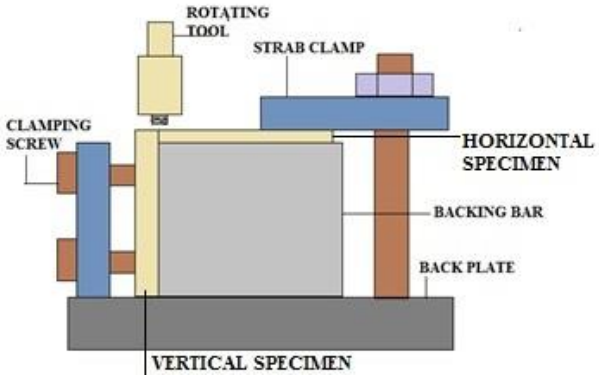

Fig. 2. Schematic diagram of FSW corner joint.

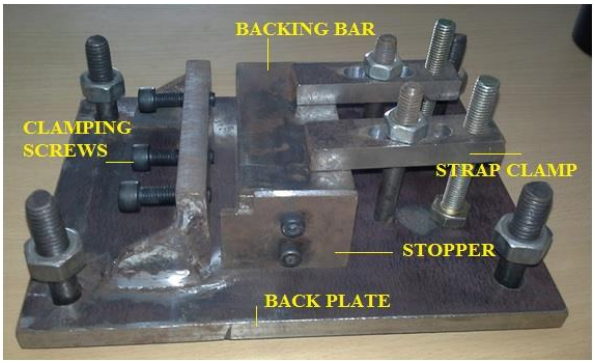

Fig. 3. Fixture for corner joints.

Three process parameters in three levels were varied, which are shown in Table 2. Taguchi L_9 orthogonal array was adopted in this work as given in Table 3. The Taguchi grey relational analysis was used to optimize the process in order to maximize the output responses, such as tensile strength and temperature distribution, and to minimize the output responses, such as microhardness, force generation and current consumption to improved quality of the weld joint. In Taguchi grey relational analysis, experimental output data are normalized in the range of zero and the multi-response problem is converted into a single response problem with the objective function. The overall performance characteristic of the multiple response processes is based on calculated grey relational grade. The percentage contribution of each parameter and prediction of optimal GRG can be primed by using ANOVA.

Table 2. FSW process parameters.

Level	Rotational speed (rev/min)	Traverse speed (mm/min)	Plunge depth (mm)
1	900	100	0.10
2	1000	150	0.20
3	1100	190	0.30

Table 3. Taguchi's L9 orthogonal array.

Exp. No.	Rotational speed (rev/min)	Traverse speed (mm/min)	Plunge depth (mm)
1	900	100	0.3
2	900	150	0.2
3	900	190	0.1
4	1000	100	0.2
5	1000	150	0.1
6	1000	190	0.3
7	1100	100	0.1
8	1100	150	0.3
9	1100	190	0.2

The FSW specimens were visually inspected for external defects post to FSW process and it was observed that the welds were free from exterior defects. The test samples were extracted from the welded plates normal to the weld line to perform the microstructural examination. The welded samples were polished and etched with standard Keller's reagent as per standard metallographic procedure. The microstructure of the weld was obtained by means of a scanning electron microscope (HITACHI-S3400N) and optical microscope (Olympus-BX61). The tensile samples were extracted from the transverse direction of the weld joint and prepared. Three samples were taken from every weld and the mean value of ultimate tensile strength (UTS) was considered for analysis. The UTS was measured using a computerized universal testing machine (INSTRON-8801). The fractured surfaces were analysed after the tensile test using a scanning electron microscope. A Vickers microhardness tester (METCO) was used for measuring the hardness across the transverse direction of the weld joint with the load of 50 g and dwell time of 15 s. The surface morphology of friction stir corner welded samples of all the nine experimental designs are shown in Fig. 4.

The weld quality parameters, such as joint efficiency, ultimate tensile strength, average hardness at the heat affected zone, stir zone and thermomechanically affected zone were measured after the FSW experiments and maximum temperature, FSW machine tool motor electrical current, force generated and temperature distributed were acquired during the experiment, which are shown in Table 4. The 6 mm thick AA5086 alloy plates were clamped vertically and 4 mm thick plate is positioned horizontally at a right angle in the FSW fixture to join dissimilar thickness plates.

Fig. 4. Surface morphology of the welded specimens: (a) Experiment 1, (b) Experiment 2, (c) Experiment 3, (d) Experiment 4, (e) Experiment 5, (f) Experiment 6, (g) Experiment 7, (h) Experiment 8, (i) Experiment 9.

Table 4. Experimental output responses.

Experimental No.	UTS (MPa)	Avg. hardness at HZ (HV)	Avg. hardness at TMAZ (HV)	Avg. hardness at SZ (HV)	Maximum temperature (°C)	Maximum force (kN)	Max. current (A)	Joint efficiency (%)
1	151	90.9	84	85.3	310	4.4	4.8	60.4
2	185	89.4	84.3	83.8	294	4.5	4.9	74
3	164	89.8	87.7	94.9	298	4.7	5.1	65.6
4	170	91.4	93.1	95.7	315	4.5	4.7	68
5	197	86.2	84.8	81.5	308	4.6	4.8	78.8
6	192	84.3	87.4	94.85	295	4.5	4.6	76.8
7	188	148.8	133.9	128.5	338	4.2	4.3	75.2
8	194	115.4	128.6	133.1	326	4.1	4.2	77.6
9	190	121.6	124.6	124.6	319	4.3	4.4	76

Optimization of FSW process parameters

In grey relational analysis (GRA), experimental output data were normalized in the range of 0 to 1. This process is called as a grey relational generation. The grey

relational coefficient was computed according to normalized value for signifying the relationship between actual experimental and the desired value. The overall grey relational grade (GRG) was calculated from the mean value the grey relational coefficients for the chosen responses. The performance characteristic of the multi-response processes computed based on grey relational grade. This procedure converts a multi-response problem into a single response optimization problem with the objective function. The last step was performing the analysis of variance to obtained percentage contribution of each parameter and prediction of optimum grey relational grade [8].

Lower the better concept was considered if the objective was to minimize the response to normalize the reference sequence using Eq. (1). Higher the better perception was considered if the objective is to maximize the response to normalize the reference sequence using Eq. (2) [8].

$$x_i(k) = \frac{\max y_i(k) - y_i(k)}{\max y_i(k) - \min y_i(k)} \tag{1}$$

$$x_i(k) = \frac{y_i(k) - \min y_i(k)}{\max y_i(k) - \min y_i(k)} \tag{2}$$

where, $x_i(k)$ are the values from grey relational generation, $miny_i(k)$ and $maxy_i(k)$ are the lower and higher value of $y_i(k)$ for the kth response, i = 1, 2, 3... the number of experiments and k= 1, 2, 3… the number of responses [8].

$$\xi_i(k) = \frac{\Delta \min + \theta \Delta \max}{\Delta_{0i}(k) + \theta \Delta \max} \tag{3}$$

where, $\Delta_{0i}(k)=\|x_0(k) - x_i(k)\|$ difference of the total value of $x_0(k)$ and $x_i(k)$; θ is the distinguishing coefficient; $0 \leq \theta \leq 1$, here θ=0.5 for all quality characteristics, Δ_{min} and Δ_{max} are the lower and higher values of $\Delta_{0i}(k)$. The mean grey relational grade (R) can be computed using Eq. (4) after averaging all the grey relation coefficients [8].

$$R_i = \frac{1}{n}\sum_{k=1}^{n} \xi_i \tag{4}$$

$$\frac{s}{n} = -10\log_{-10}\left(\frac{1}{n}\sum_{i=1}^{n}\frac{1}{R_{ij}^2}\right) \tag{5}$$

where n is the number of responses.

3. Results and Discussion

3.1. Selection of optimal parameters setting with Taguchi GRA

In this investigation, Taguchi grey relational analysis is preferred for selected optimal parameter settings. The output responses such as ultimate tensile strength, maximum temperature distribution and joint efficiency were normalized using 'higher the better' criteria using Eq. (2). The maximum current consumption, maximum force generation and average hardness values at SZ, TMAZ and HAZ were normalized using 'lower the better' criteria the Eq. (1).

The objective is to maximize the ultimate tensile strength, temperature distribution and joint efficiency at the same time minimizing the downforce, current

and microhardness values. The normalized data are quantified as shown in Table 5. The grey relational coefficient was computed using the Eq. (3) and grey relational grades (GRG) was computed using Eq. (4). In this stage, multi-performance characteristics changed into a single GRG value. The standard deviation for normalized values is shown in Table 6. The GRG values and related S/N ratio of all the experiments are given in Table 7. The GRG values vary between 0 and 1.

Table 5. Normalized values of output responses.

Experimental No.	UTS (MPa)	Avg. hardness at HZ (HV)	Avg. hardness at TMAZ (HV)	Avg. hardness at SZ (HV)	Maximum temperature (°C)	Maximum force (kN)	Max. current (A)	Joint efficiency (%)
1	0.00	0.898	1.000	0.926	0.484	0.33	1.000	0.000
2	0.73	0.921	0.994	0.955	0.258	0.16	0.857	0.739
3	0.28	0.915	0.926	1.000	0.000	0.00	0.857	0.283
4	0.41	0.890	0.818	0.089	0.645	0.50	0.714	0.413
5	1.00	0.971	0.984	0.000	0.548	0.50	0.571	1.000
6	0.89	1.000	0.932	0.164	0.387	0.66	0.714	0.891
7	0.80	0.000	0.000	0.725	1.000	1.00	0.429	0.804
8	0.93	0.518	0.106	0.740	0.790	0.83	0.429	0.935
9	0.84	0.422	0.186	0.741	0.613	0.66	0.000	0.848

Table 6. Standard deviation.

Experimental no.	SD in UTS (MPa)	SD in avg. hardness at HAZ (HV)	SD in avg hardness at TMAZ (HV)	SD in avg. hardness in SZ (HV)	SD in maximum temperature (°C)	SD in maximum force (kN)	SD in maximum current (A)	SD in joint efficiency (%)
1	1.000	0.102	0.000	0.074	0.636	0.500	0.667	1.000
2	0.261	0.079	0.006	0.045	1.000	0.667	0.778	0.261
3	0.717	0.085	0.074	0.260	0.909	1.000	1.000	0.717
4	0.587	0.110	0.182	0.275	0.523	0.667	0.556	0.587
5	0.000	0.029	0.016	0.000	0.682	0.833	0.667	0.000
6	0.109	0.000	0.068	0.259	0.977	0.667	0.444	0.109
7	0.196	1.000	1.000	0.911	0.000	0.167	0.111	0.196
8	0.065	0.482	0.894	1.000	0.273	0.000	0.000	0.065
9	0.152	0.578	0.814	0.836	0.432	0.333	0.222	0.152

Table 7. Grey relational grades with corresponding S/N ratios and rank.

Experimental no.	GRG	S/N ratio	Rank
1	0.592	-4.55178	6
2	0.655	-3.6797	4
3	0.528	-5.5426	9
4	0.564	-4.9812	8
5	**0.767**	**-2.2985**	**1**
6	0.685	-3.2887	3
7	0.628	-4.0360	5
8	0.702	-3.0710	2
9	0.573	-4.8431	7

The results of the analysis of variance are shown in Table 8. The traverse speed has the highest contribution of 54.31% on the total variability, next rotation speed with 20.52% and plunging depth with 13.25%, which means the rotation speed, has the highest response. In addition, the contribution of the error was 11.91%. The mean S/N ratio for each parameter at various levels computed and is shown in Table 9.

The main effect plot of input process parameters on GRG is given in Fig. 5. According to the main effect plot, the optimum set of process parameters for multi-response optimization problem was obtained at level 2 of tool rotation speed, level 2 of traverse speed and level 1 of plunge depth. Response table for S/N ratio and grey relational grade is given in Tables 9 and 10 respectively.

The optimum set of parameters obtained as traverse speed of 150 mm/min, tool rotation speed of 1000 rev/min, and plunge depth of 0.1 mm. Therefore, it can be concluded that the traverse speed was the main influencing factor, followed by the rotation speed and plunging depth.

Table 8. Analysis of variance for grey relational grades.

Source	DF	Sum of squares	Mean sum	F-value	Probability significance	% of contribution
Rotation speed	2	0.00967	0.0048	1.72	0.367	20.52
Traverse speed	**2**	**0.02561**	**0.0128**	**4.56**	**0.180**	**54.31**
Plunging depth	2	0.00625	0.0031	1.11	0.473	13.25
Error	2	0.00561	0.0028			11.91
Total	8	0.0471				

Table 9. Response table for S/N ratio of grey relational grades.

Level	Rotational speed	Traverse speed	Plunging depth
1	-4.591	-4.523	-3.637
2	-3.523	-3.016	-4.501
3	-3.983	-4.558	-3.959
Delta	1.069	1.542	0.864
Rank	2	1	3

Table 10. Response table for grey relational grades.

Level	Rotational speed	Traverse speed	Plunging depth
1	0.591	0.594	0.659
2	0.671	0.708	0.596
3	0.634	0.595	0.641
Delta	1.069	1.542	0.864
Rank	1	2	3

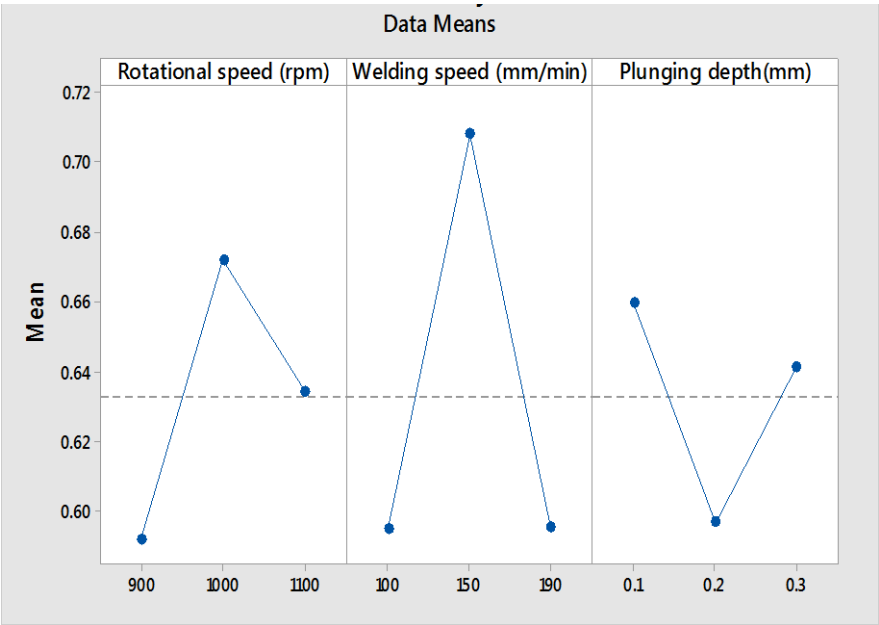

Fig. 5. Main effect plot for GRG.

3.2. Microstructure of corner FSW specimens

Figures 6 to 8 illustrate the optical micrographs of the cross-sections of weld samples normal to weld line. Three different zones, such as Heat Affected Zone (HAZ), Thermomechanically Affected Zone (TMAZ), and Stir Zone (SZ) have been recognized. Figures 6 to 8(a) demonstrate the microstructure of parent material. Figures 6 to 8(b) demonstrate the microstructure of heat affected zones. It was hard to find the difference in grain structure of parent material and heat affected zone because of low thermal affectability.

Figures 6 to 8(c) show the microstructure of the thermomechanically affected zones. The boundary between thermomechanically affected zone and stir zone can be seen clearly. Thermomechanically affected zone and heat affected zone developed the transition zone. Thermomechanically affected zone represents highly stretched grains of the aluminium alloy without recrystallization. Both sides of the thermomechanically affected zone revealed a similar microstructure. The thermomechanically affected zone was thermally affected and deformed plastically not recrystallized.

Figures 6 to 8(d) reveal the microstructure of the stir zone. The stir zone experienced the high temperature and the heavy plastic deformation. The heavy plastic deformation produced fine-equiaxed recrystallized grains in stir zone followed by dynamic recrystallization. The frictional heat produced during welding was the reason for refinement of grain in the weld zone, which could improve the strength of the weld. The defects of fusion welding such as porosity, slag inclusion, and voids were not found in the weld zone [9-11].

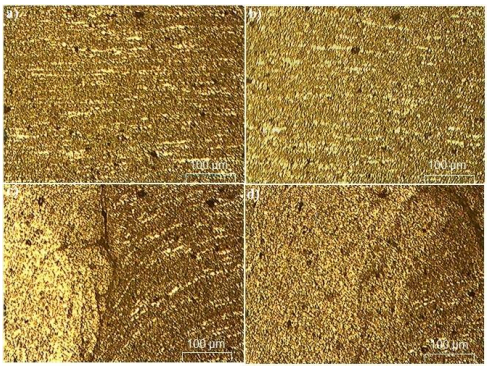

Fig. 6. Optical micrographs of friction stir weld at rotational and traverse speeds of 1000 rev/min and 100 mm/min: (a) Parent metal AA5086, (b) Heat affected zone, (c) Thermomechanically affected zone, (d) Weld zone.

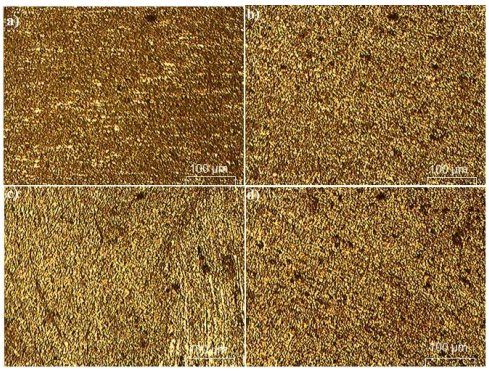

Fig. 7. Optical micrographs of friction stir weld at rotational and traverse speeds of 1000 rev/min and 150 mm/min: (a) Parent metal AA5086, (b) Heat affected zone, (c) Thermomechanically affected zone, (d) Weld zone.

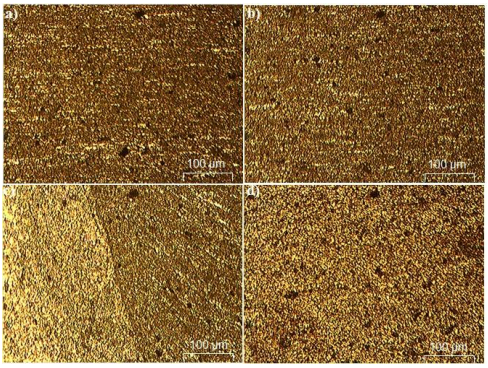

Fig. 8. Optical micrographs of FSW specimen. (Rotational speed of 1000 rev/min and traverse speeds of 190 mm/min): (a) Parent metal AA5086, (b) Heat affected zone, (c) Thermomechanically affected zone, (d) Weld zone.

3.3. SEM analysis of corner FSW specimen

Figure 9(a) illustrates the microstructure of the parent material. Figures 9(b) to (d) show SEM micrographs of the stir zone of the joint welded at a rotational speed of 1000 rev/min and traverse speeds of 100 mm/min, 150 mm/min and 190 mm/min. Figures 9(b) to (d) show the stir zones included fine equiaxed grains is attributed to the dynamic recrystallization because of frictional heat and plastic deformation produced by the rotating tool. Figure 9(d) shows broken precipitates present in the stirred zone because of severe deformation of the material during the FSW process. It is observed from Fig. 9(c) that the weld zone, fabricated at a rotational speed of 1000 rev/min and traverse speed of 150 mm/min included finer grains than the other joints and yielded higher tensile strength. The average grain size in the weld zone was 12 to 15μm, which were much smaller than the base material. The grain size of the weld zone reduced with increasing traverse speed [12-15].

3.4. Fractographs

Figure 10 illustrates SEM micrographs of the fractured surface after the tensile test, fabricated at the traverse speed of 150 mm/min and the rotational speed of 1000 rev/min with different scales. Figures 10(b) and (c) show the fracture surfaces formed with a huge number of microscopic voids that varies in shape and size. Figure 10(d) demonstrates the large-scale view of the fractured surface that signifies a homogeneously rough surface. The ductile fractured feature with voids nucleation and coalescence is observed in the enlarged view of the fractured surface. A large quantity of dimples with various depths represents that a ductile fracture occurred in these regions. These dimples are responsible for fracture at the heat-affected zone [16-20].

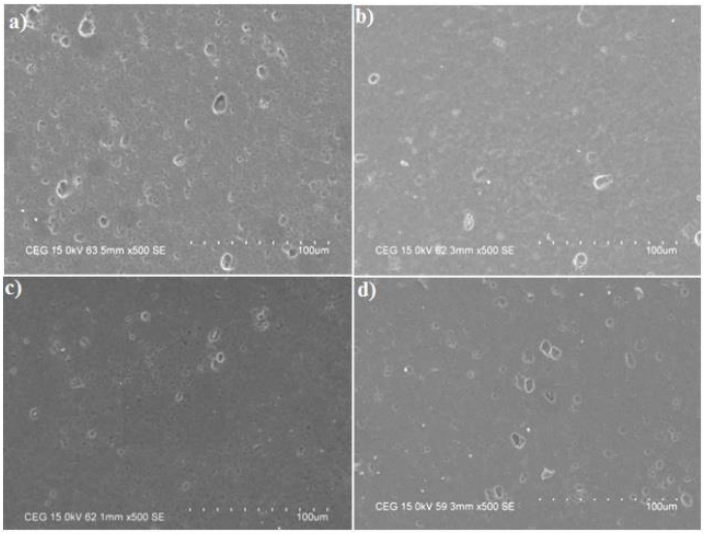

Fig. 9. SEM micrographs of FSW specimen: (a) Base metal, (b) Weld zone at traverse speeds of 100 mm/min, (c) Weld zone at traverse speed of 150 mm/ min and (d) Weld zone at traverse speed of 190 mm/min.

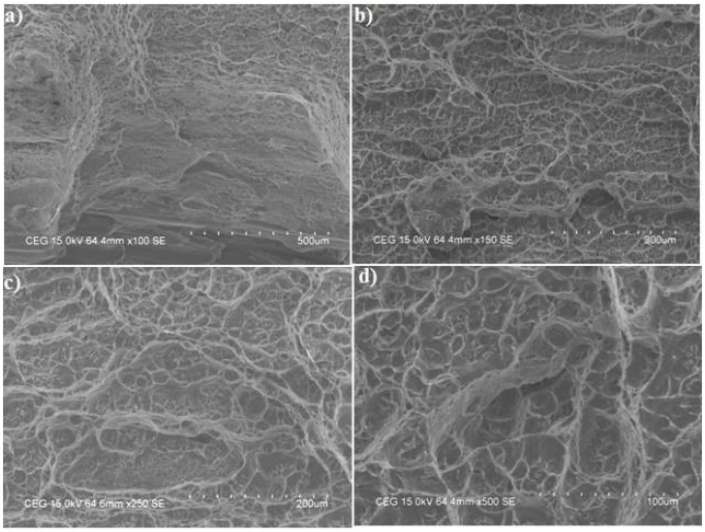

Fig. 10. Fractographs with different scale of FSW tensile test specimen produced at welding speed of 150 mm/min and the rotational speed of 1000 rev/min.

4. Conclusions

The multiple performance characteristics of FSW of AA5086 aluminium alloy corner joints were optimized using Taguchi Grey Relational Analysis. The following conclusions were drawn from the experimental analysis and optimization process:

- The analysis brought the optimized process parameters, the traverse speed of 150 mm/min, the rotational speed of 1000 rev/min, and plunge depth of 0.10 mm for corner FSW of AA5086 aluminium alloy.
- Based on the ANOVA results of grey relational grade, the percentage contribution of the traverse speed is 54%, which revealed a significant influence on multi-response, and rotational speed of 21% and plunge depth of 13%.
- The ultimate tensile strength of 197 MPa was obtained, which is 78% of the base material. A lower tensile strength of 151 MPa was attained, which is 60% of the base metal.
- A maximum microhardness of 157 HV was obtained at stir zone of the joint due to significant grain refinement, which is higher than the parent material.
- The fracture positions of all joints located at heat affected zone that indicate defect free stir zone. The peak temperature of 338° C obtained at a rotational speed of 1100 rev/min and traverse speed of 100 mm/min.
- The downward force reaches the peak value of 4.7 kN during plunging of the tool shoulder on the surface of the material. Then force reduced significantly and remains a steady state value of 4.1 kN during the translational stage until the tool departures the work plate material.

Nomenclatures

I	Number of experiments
k	Number of responses
n	Number of process responses
R_i	Grey relational grade
x_i	Normalised values

Greek symbols

Δ	Standard deviation
θ	Distinguishing coefficient
ξ_i	Grey relational coefficient

Abbreviations

AA	Aluminium Alloy
ANOVA	Analysis of Variance
FSW	Friction Stir Welding
GRA	Grey Relational Analysis
GRC	Grey Relational Coefficient
GRG	Grey Relational Grade
HAZ	Heat Affected Zone
S/N	Signal to Noise
SD	Standard Deviation
SZ	Stir Zone
TMAZ	Thermomechanically Affected Zone
TWI	The Welding Institute
UTS	Ultimate Tensile Strength

References

1. Yan, Y.; Zhang, D.-t; Qui, C.; and Zhang, W. (2010). Dissimilar friction stir welding between 5052 aluminium alloy and AZ31 magnesium alloy. *Transactions of Nonferrous Metals Society of China*, 20(2), 619-623.
2. Ilangovan, M.; Boopathy, S.R.; and Balasubramanian, V. (2015). Effect of tool pin profile on microstructure and tensile properties of friction stir welded dissimilar AA6061-AA5086 aluminium alloy joints. *Defence Technology*, 11(2), 174-184.
3. Palanivel, R.; Mathews, P.K.; Dinaharan, I.; and Murugan, N. (2014). Mechanical and metallurgical properties of dissimilar friction stir welded AA5083-H111 and AA6351-T6 aluminium alloys. *Transactions* of *Nonferrous Metals Society of China*, 24(1), 58-65.
4. Ahmed, M.M.Z.; Ataya, S.; El-Seyed Seleman, M.M.; Ammar, H.R.; and Ahmed, E. (2014). Friction stir welding of similar and dissimilar AA7075 and AA5083. *Journal of Material Processing Technology*, 242, 77-91.

5. Martin, J.P.; Stanhope, C.; and Gascoyne, S. (2011). Novel techniques for corner joints using friction stir welding. *Proceedings of the TMS Annual Meeting & Exhibition*. San Diego, California, United States of America, 177-186.
6. Palanivel, R.; and Mathew, P.K. (2012). Prediction and optimization of process parameter of friction stir welded AA5083-H111 aluminium alloy using response surface methodology. *Journal of Central South University*, 19(1), 1-8.
7. Casalino, G.; Campanelli, S.; and Mortello, O. (2014). Influence of shoulder geometry and coating of the tool on the friction stir welding of aluminium alloy plates. *Proceedings of the 24th DAAAM International Symposium on Intelligent Manufacturing and Automation.* Bari, Italy, 1541-1548.
8. Sahu, P.K.; and Pal, S. (2015). Multi-response optimization of process parameters in friction stir welded AM20 magnesium alloy by Taguchi grey relational analysis. *Journal of Magnesium and Alloys*, 3(1), 36-46.
9. Dinaharan, I.; and Murugan, N. (2012). Effect of friction stir welding on microstructure, mechanical and wear properties of AA6061/ZrB_2 in-situ cast composites. *Materials Science and Engineering A*, 543, 257-266.
10. Li, X,-w.; Zhang, D.-t.; Qiu, C.; and Zhang, W. (2012). Microstructure and mechanical properties of dissimilar pure copper/1350 aluminium alloy butt joints by friction stir welding. *Transactions of Nonferrous Metals Society of China*, 22(6), 1298-1306.
11. Aval, H.J. (2015). Influences of pin profile on the mechanical and microstructural behaviours in dissimilar friction stir welded AA6082-AA7075 butt joint. *Materials and Design*, 67, 413-421.
12. Akinlabi, E.T.; Andrews, A.; and Akinlabi, S.A. (2014). Effects of processing parameters on corrosion properties of dissimilar friction stir welds of aluminium and copper. *Transactions of Nonferrous Metals Society of China*, 24(5), 1323-1330.
13. Ahn, B.-W.; Choi, D.-H.; Kim, Y,-H.; and Jung, S.-B. (2012). Fabrication of SiCp/AA5083 composite via friction stir welding. *Transactions of Nonferrous Metals Society of China*, 22, 634-638.
14. Dawood, H.I.; Mohammed, K.S.; Rahmat, A.; and Uday, M.B. (2015). Effect of small tool pin profiles on microstructures and mechanical properties of 6061 aluminium alloy by friction stir welding. *Transactions of Nonferrous Metals Society of China*, 25(9), 2856-2865.
15. Dorbane, A.; Mansoor, B., Ayoub, G.; Shunmugasamy, V.C.; and Imad, A. (2016). Mechanical, microstructural and fracture properties of dissimilar welds produced by friction stir welding of AZ31B and Al6061. *Materials Science and Engineering*, 651, 720-733.
16. Khan, N.Z.; Siddiquee, A.N.; Khan, Z.A.; and Mukhopadhyay, A.K. (2017). Mechanical and microstructure behaviour of friction stir welded similar and dissimilar sheets of AA2219 and AA7475 aluminium alloys. *Journal of Alloys and Compounds*, 695(C), 2902-2908.
17. Chao, Y.J.; Qi, X.; and Tang, W. (2003). Heat transfer in friction stir welding-experimental and numerical studies. *Journal of Manufacturing Science and Engineering*, 125(1), 138-145.

18. Trimble, D.; Monaghan, J.; and O'Donnell, G.E. (2012). Force generation during friction stir welding of AA2024-T3. *Manufacturing Technology*, 61(1), 9-12.
19. Senthil Kumar, S.; Ashok, S.D.; and Narayanan, S. (2013). Investigation of friction stir butt welded aluminium alloy flat plates using spindle motor current monitoring method. *Proceedings of the International Conference on Design and Manufacturing (IConDM)*, Chennai, India, 915-925.
20. Buffa, G.; Campanella, D.; Lorenzo, R.D.; Fratini, L.; and Ingarao, G. (2017). Analysis of electrical energy demands in friction stir welding of aluminium alloys. *Proceedings of the 17th International Conference on Sheet Metal (SHEMET17)*. Palermo, Italy, 206-212.